Supporting information for

Deciphering the Stimuli-Responsive Behavior of TPPE-Incorporated Flexible Metal-Organic Frameworks

You Fan [a, c], Zhikai Zhu [c], Shuo Zhou [c], Federico Gorelli [c], Yuchen Ye [c], Huixin Hu [c], Shenghan Zhang [c], Hongliang Dong [c], Changzhong Liao[a, *], Ziyou Zhang[b, c, *], Zhiqiang Chen [c, *]

[a] School of Resources, Environment and Materials, Guangxi University, Nanning 530004, China

[b] School of Chemistry and Chemical Engineering, Fuyang Normal University, Fuyang 236041, PR China

[c] Center for High Pressure Science and Technology Advanced Research, Shanghai, 201203, China.

* Corresponding author:

*Email: liaocz29@connect.hku.hk (C.Z.L.);

ziyou.zhang@fynu.edu.cn (Z.Y.Z.);

chenzq@hpstar.ac.cn (Z.Q.C.).

1. Methods

Synthesis of D-MOF

All reagents and solvents were commercially obtained and used without further purification. D-(+)-camphoric acid (D-H_2Cam, 98%, Energy Chemical), (TPPE, 98%, Extension), cadmium nitrate tetrahydrate ($Cd(NO_3)_2 \cdot 4H_2O$, 99%, Energy Chemical), N,N'-dimethylformamide (DMF, 99.9%, Energy Chemical), methanol (99.5%, Beijing Chemical Works), ethanol (99.5%, Beijing Chemical Works), deionized water (Mini Q, 18.2 MΩ·cm). D-H_2Cam (20 mg, 10 mmol) and TPPE (32 mg, 5 mmol) were dissolved in 8 mL of DMF/ethanol (6:2 mL) and sonicated for 10 min to ensure homogeneous dispersion. $Cd(NO_3)_2 \cdot 4H_2O$ (30.8 mg) was dissolved in deionized water (2 mL) prior to use, and the resulting aqueous solution was added into the above dispersion and then the mixture was sonicated for an additional 15 min. The resulting solution was transferred into a 15 mL glass vial and heated at 95 °C for 24 h in an oil bath. After completion of the reaction, the glass vial was cooled to room temperature, and the resulting crystals were collected, washed with DMF, and vacuum-dried for 12 h to yield of colorless transparent D-MOF crystals (29.2 mg, 46% based on Cd). Element analysis: calculated C, 62.86%; H, 4.76%; N, 4.44%; found C, 62.93%; H, 4.72%; N, 4.41%.

High pressure generation

High pressure was applied using a diamond anvil cell (DAC) equipped with a pair of type-IIa symmetric diamond anvils in 300 μm culet size. A T301 stainless steel gasket was pre-indented to ~40 μm in thickness, and a ~150 μm hole was laser-drilled at its

center to form the sample chamber. KBr was selected as the pressure transmission medium (PTM) for infrared measurements, whereas silicone oil was used in all other in-situ high-pressure experiments. Pressure was calibrated using the ruby fluorescence method.[1] All measurements were conducted at ambient temperature.

In-situ high-pressure measurements

In-situ high-pressure fluorescence spectra were carried out on a multifunctional optical platform, employing a 360 nm laser (1 mW) as the excitation source, with a laser spot size of approximately 10 μm.

Time-resolved photoluminescence (TRPL) measurements were performed using a 405 nm laser with a pulse width of 20 ps and a repetition rate of 4 MHz.

In-situ high-pressure UV-Vis absorption spectra were acquired on a custom-designed micro-area spectroscopic system (Gora-UVN-FL, assembled by Ideaoptics) equipped with a Mitutoyo 20× NUV objective, using a deuterium/halogen light source covering 300 nm – 1100 nm.

In-situ high-pressure infrared spectra were collected on a Bruker Vertex 70 v FT-IR spectrometer (Bruker Optik GmbH, Germany) equipped with a nitrogen-cooled mercury cadmium telluride (MCT) detector.

In-situ high-pressure Raman spectra were recorded on a laser confocal scanning Raman/luminescence microscope (HORIBA Jobin Yvon) using an 830 nm excitation source and a 1200 $g \cdot mm^{-1}$ grating.

Element Analysis

Elemental analysis for C/H/N was performed in a Euro Vector EA3000 element

analyzer.

Powder X-ray structural determination

The MOF crystals were directly put onto a single-crystal silicon wafer (zero-background holder) to record the X-ray diffraction spectra on Malvern Panalytical Empyrean X-ray diffractometer with Cu/K α radiation (λ = 1.5406Å, 40 KV, 40 mA).

Single crystal X-ray structural determination

Single-crystal X-ray diffraction (SCXRD) data were collected at beamline BL17B of the National Facility for Protein Science in Shanghai (NFPS) and Shanghai Advanced Research Institute, CAS, using a wavelength of 0.6888 Å. The crystal structures were solved by direct methods and refined by full-matrix least-squares refinements based on F^2 using the SHELXTL program.[2-4] Non-hydrogen atoms were refined anisotropically, while the hydrogen atoms were placed in their geometrically ideal positions and refined isotropically. Except for hydrogen atoms of water molecules, all others were generated geometrically and refined isotropically using the riding model.

Methods of Calculation

Density functional theory (DFT) calculations were performed using the Dmol3 package in Materials Studio 8.0.[5,6] Exchange energy and correlation energy were treated with the nonlocal generalized gradient approximation (GGA) of the Perdew-Burke-Ernzerhof (PBE) correlation functional.[7] The convergence thresholds for geometry optimization were set as follows: 2.0×10^{-5} Ha for energy, 0.004 Ha/Å for maximum force, 0.005 Å for maximum displacement, and 1.0×10^{-6} Ha for self-consistent field (SCF) for all atoms. A cutoff energy of 400 eV was applied to the plane-

wave basis set. The excited-state calculations were performed using time-dependent density functional theory (TD-DFT)[8] as implemented in the CP2K package[9] based on the optimized structures. The first 20 excited states were calculated using the B3LYP functional with the 6-311G(d,p) basis set, together with the D3 dispersion correction. The resulting wavefunction files were further analyzed using Multiwfn 3.6[10,11] to extract the relevant electronic structure information and perform electron–hole analysis. The electron and hole distributions as well as charge density difference maps were visualized and rendered using VESTA[12].

2. Supplemental Tables

Table S1. Fitted time-resolved PL decay curves of D-MOF during the compression and decompression. D for decompression.

Function name	ExpDec2					
Formula	$y = y_0 + A_1 \times \exp(-x/t_1) + A_2 \times \exp(-x/t_2)$					
Pressure (GPa)	y_0	A_1	t_1	A_2	t_2	R^2 (COD)
1 atm	1.76×10^{-3}	0.6071	0.70528	0.40617	2.27732	0.99974
0.5	3.11×10^{-4}	0.53614	0.49529	0.48395	1.94468	0.99957
0.7	3.37×10^{-4}	0.59087	0.37713	0.44319	1.71474	0.99945
2.0	4.13×10^{-4}	0.70573	0.31483	0.34441	1.59751	0.99919
3.3	4.60×10^{-4}	0.77335	0.27085	0.2773	1.44418	0.99899
4.0	5.14×10^{-4}	0.8603	0.26349	0.22685	1.43679	0.99831
6.5	7.55×10^{-4}	0.99581	0.21281	0.13463	1.38908	0.9969
7.8	8.90×10^{-4}	1.00933	0.20129	0.11699	1.38523	0.99658
9.2	1.11×10^{-3}	0.9964	0.17952	0.10855	1.30057	0.99714
D 8.4	1.81×10^{-3}	1.10332	0.17228	0.08103	1.37942	0.99479
D 6.2	1.74×10^{-3}	1.04072	0.1779	0.08905	1.39615	0.99567
D 4.1	1.88×10^{-3}	1.0034	0.18912	0.11524	1.51948	0.99639
D 1.9	2.81×10^{-3}	0.80344	0.27027	0.27415	1.90373	0.99837
D 1.2	2.86×10^{-3}	0.72756	0.29339	0.31994	1.93602	0.99888
D 0.3	2.56×10^{-3}	0.54936	0.46493	0.47529	2.24123	0.99947
D 1 atm	2.71×10^{-3}	0.337	0.94764	0.65925	3.26143	0.99981

Table S2. Comparison of crystallographic parameters for D-MOF single-crystal before and after pressure treatment.

	Original	**Released**
Formula	$C_{33}H_{30}CdN_2O_4$	$C_{66}H_{96}Cd_2N_4O_{26}$
Crystal system	hexagonal	trigonal
Space group	$P6_222$	$P3_221$
a (Å)	16.5556 (2)	16.657 (4)
b (Å)	16.5556 (2)	16.657 (4)
c (Å)	47.8604 (9)	47.635 (16)
α (°)	90	90
β (°)	90	90
γ (°)	120	120
V (Å^3)	11360.5 (3)	11446 (6)
Z	/	6
D_c, g·cm^{-3}	/	1.381
μ, mm^{-1}	/	0.634
F(000)	/	4944.0
R_{int}	/	0.0843
R_1[a] ($I > 2\sigma(I)$)	/	0.0598
wR_2[b] (all data)	/	0.1397
R_1 (all data)	/	0.0782
wR_2 (all data)	/	0.1492
GOF	/	1.059

$R_1 = \Sigma\|F_o| - |F_c\|/\Sigma|F_o|$. $wR_2 = |\Sigma w(|F_o|^2 - |F_c|^2)/\Sigma|w(F_o)^2|^{1/2}$.

Table S3. Selected Bond length (Å) and bond angles (°) for **D-MOF** after pressure.

Cd1—N1	2.308 (11)	Cd1—O6	2.412 (10)
Cd1—O1	2.247 (11)	Cd1—O5	2.237 (11)
Cd1—O2	2.401 (10)	Cd1—N2[1]	2.296 (11)
Cd2—O3[2]	2.352 (9)	Cd2—O4[2]	2.302 (10)
Cd2—O7	2.295 (10)	Cd2—O8	2.323 (9)
Cd2—N3	2.309 (10)	Cd2—N4[3]	2.291 (10)
N1—Cd1—O2	85.7 (4)	N1—Cd1—O6	112.3 (4)
O1—Cd1—N1	139.6 (4)	O1—Cd1—O2	55.2 (3)
O1—Cd1—O6	108.0 (4)	O1—Cd1—N2[1]	96.7 (6)
O2—Cd1—O6	155.5 (4)	O5—Cd1—N1	98.0 (4)
O5—Cd1—O1	103.1 (4)	O5—Cd1—O2	108.0 (4)
O5—Cd1—O6	54.9 (4)	O5—Cd1—N2[1]	138.3 (5)
N2[1]—Cd1—N1	89.5 (6)	N2[1]—Cd1—O2	113.5 (5)
N2[1]—Cd1—O6	84.2 (5)	O3[2]—Cd2—O8	97.4 (3)
O4[2]—Cd2—O3[2]	55.4 (3)	O4[2]—Cd2—O8	99.7 (4)
O4[2]—Cd2—N3	113.9 (4)	O7—Cd2—O3[2]	99.3 (4)
O7—Cd2—O4[2]	144.2 (3)	O7—Cd2—O8	54.9 (3)
O7—Cd2—N3	90.1 (4)	N3—Cd2—O3[2]	93.1 (3)
N3—Cd2—O8	144.7 (4)	N4[3]—Cd2—O3[2]	145.6 (4)
N4[3]—Cd2—O4[2]	90.5 (3)	N4[3]—Cd2—O7	113.4 (4)
N4[3]—Cd2—O8	92.9 (3)	N4[3]—Cd2—N3	97.2 (3)

Symmetry codes: *[1]+X,1+Y,+Z; [2]1-X,-X+Y,2/3-Z; [3]1+X,+Y,+Z.*

Table S4. The dihedral angles of TPPE in D-MOF before and after pressure treatment.

	Original		**Released**	
	P1-P2 (deg)	P2-P3 (deg)	P1-P2 (deg)	P2-P3 (deg)
1	56.12	27.64	55.32	25.66
2	56.12	27.64	55.32	25.66
3	56.20	27.64	56.66	26.45
4	56.20	27.64	56.66	26.45
Average	56.16	27.64	55.99	26.06

3. Supplemental Figures

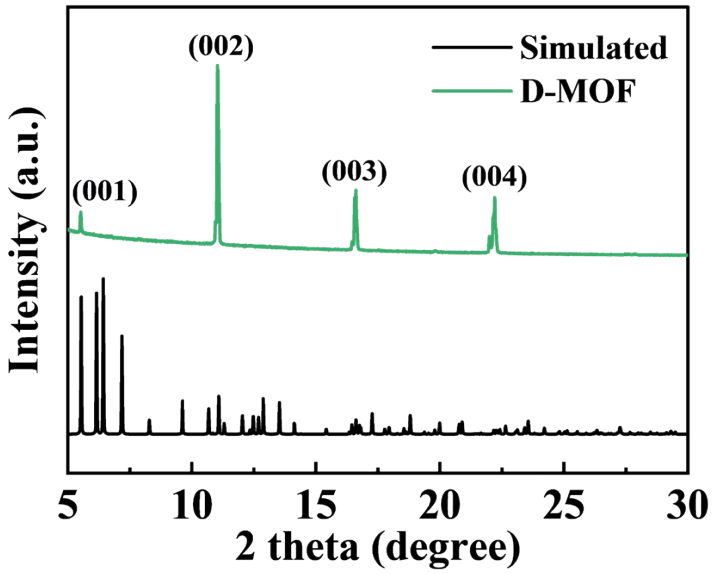

Figure S1 The powder XRD spectra and the simulated powder XRD spectra from the single crystal of D-MOF

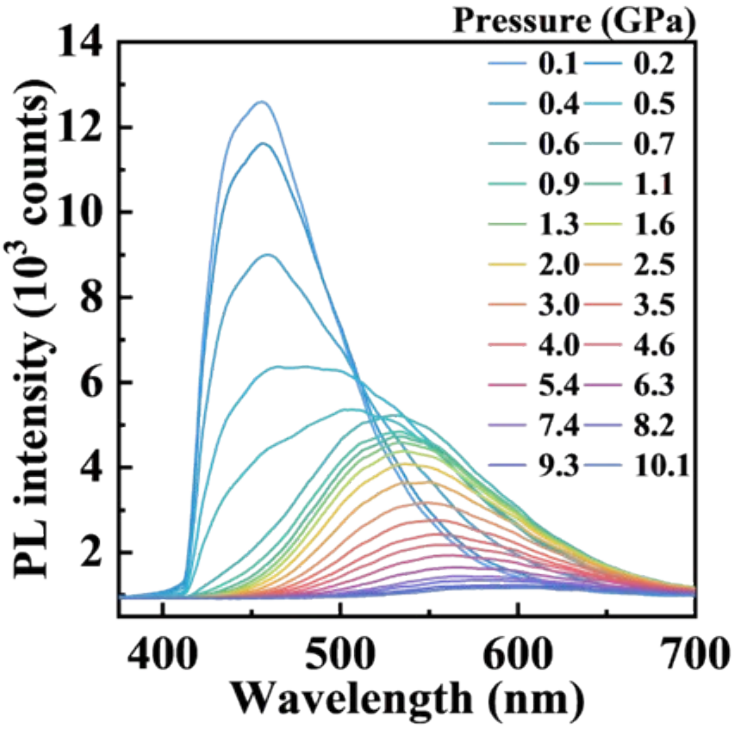

Figure S2 In-situ high-pressure PL spectra of D-MOF during compression.

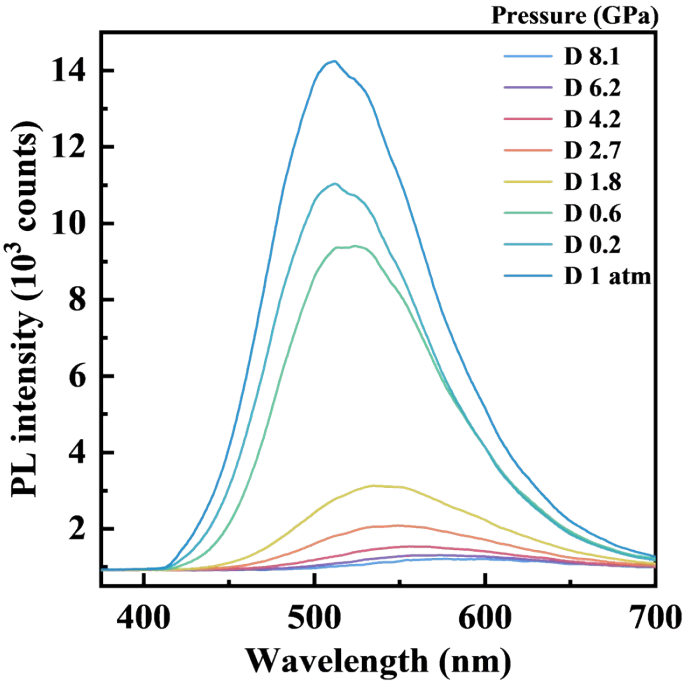

Figure S3. In-situ high-pressure PL spectra of D-MOF during decompression. D for decompression.

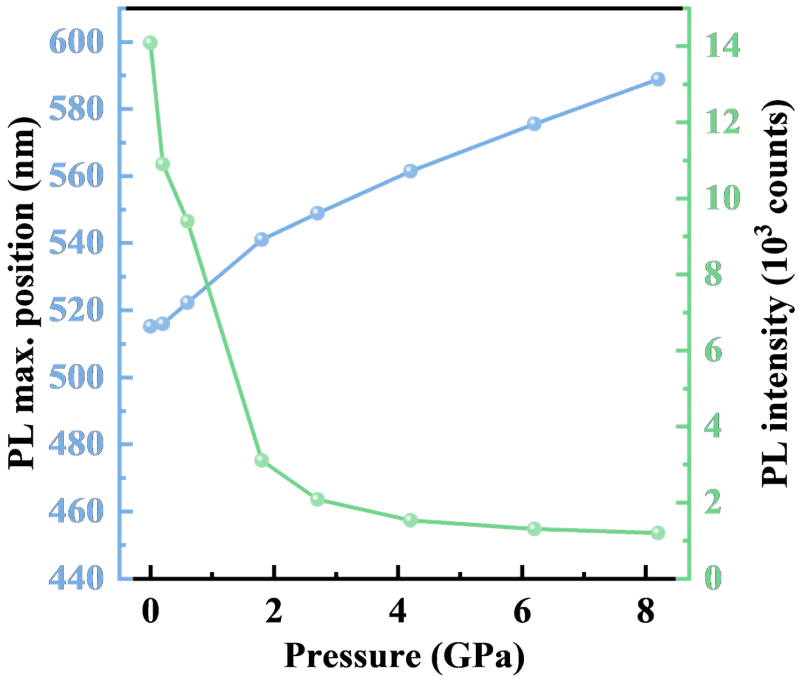

Figure S4. Pressure-dependent evolution of PL intensity and emission wavelength of D-MOF released from 10.1 GPa.

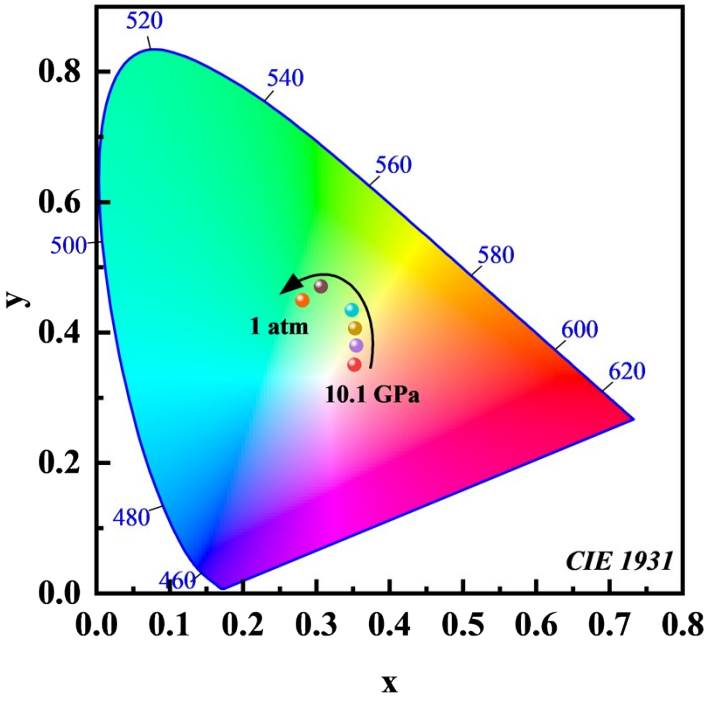

Figure S5. CIE chromaticity diagram of D-MOF during decompression.

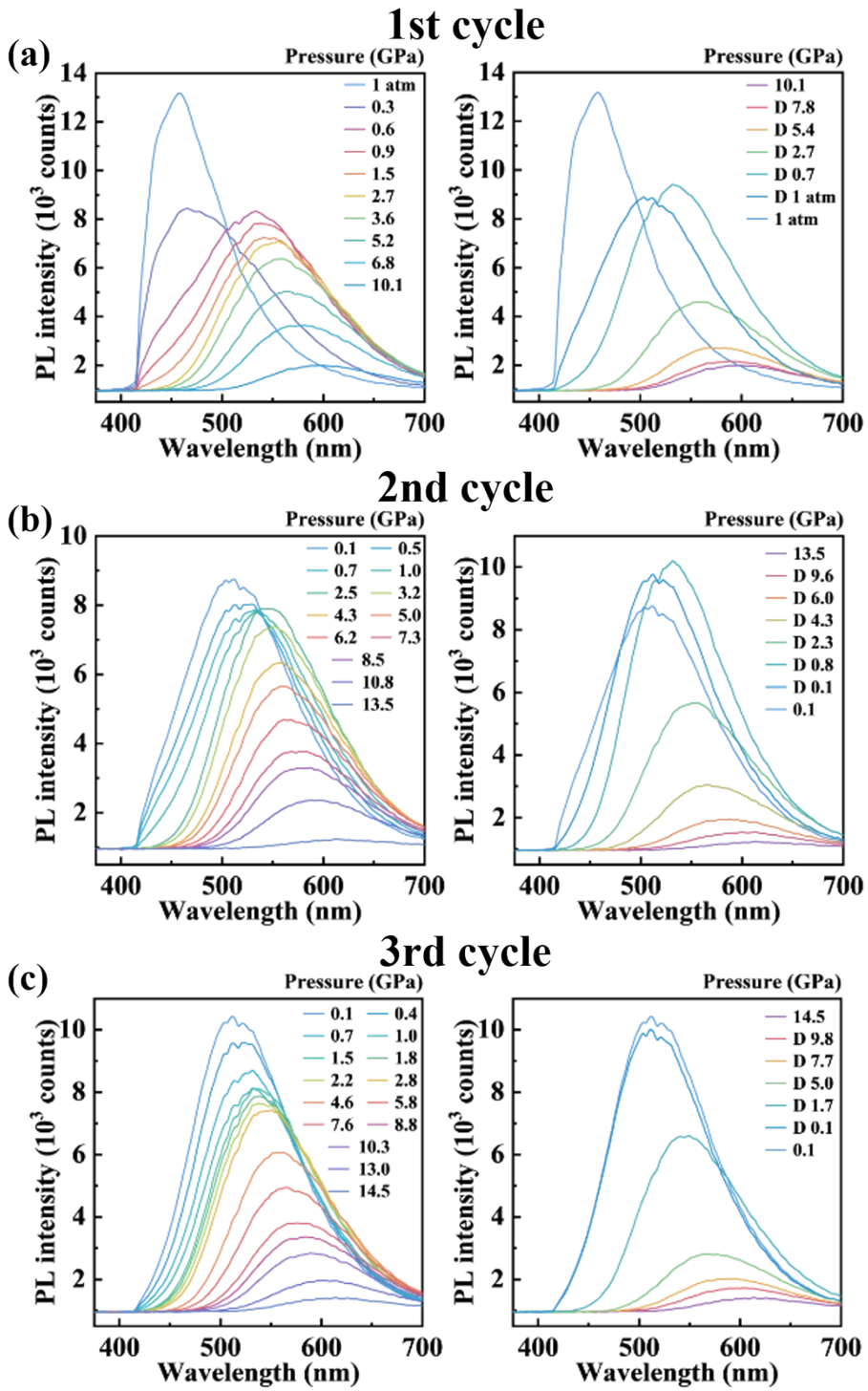

Figure S6. In-situ high-pressure PL spectra of D-MOF during three consecutive compression-decompression cycles.

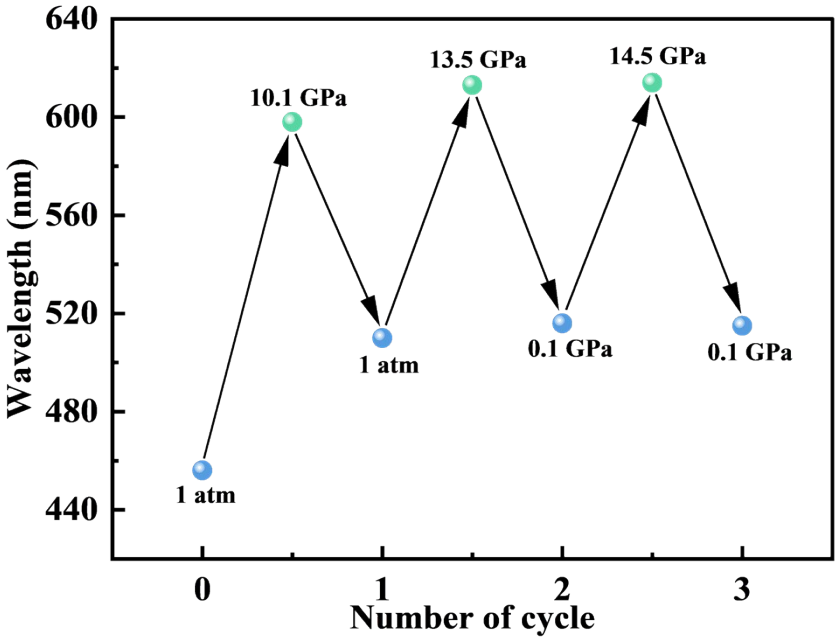

Figure S7. Evolution of the fluorescence emission wavelength of D-MOF over three compression-decompression cycles.

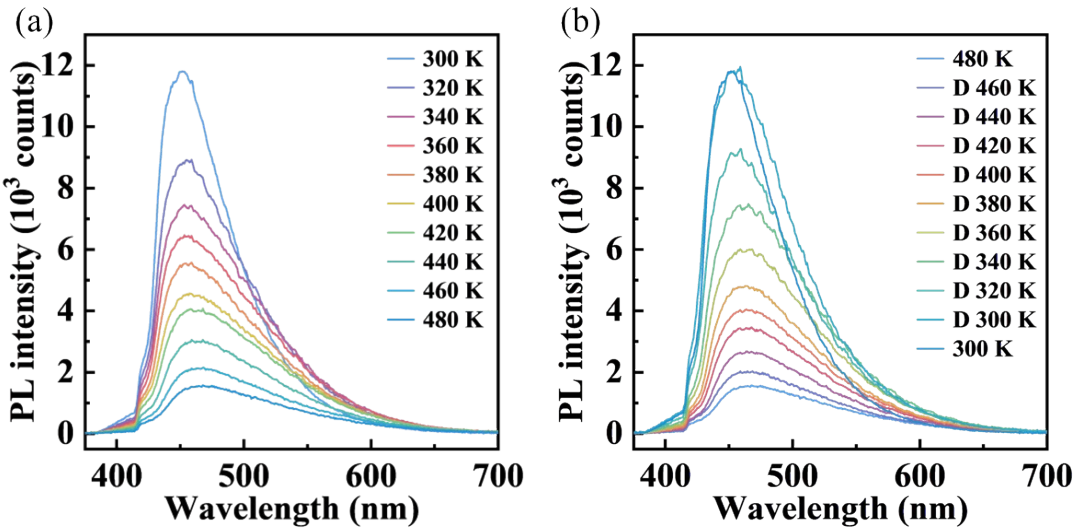

Figure S8. Temperature-dependent PL spectra of D-MOF during heating (a) and cooling (b).

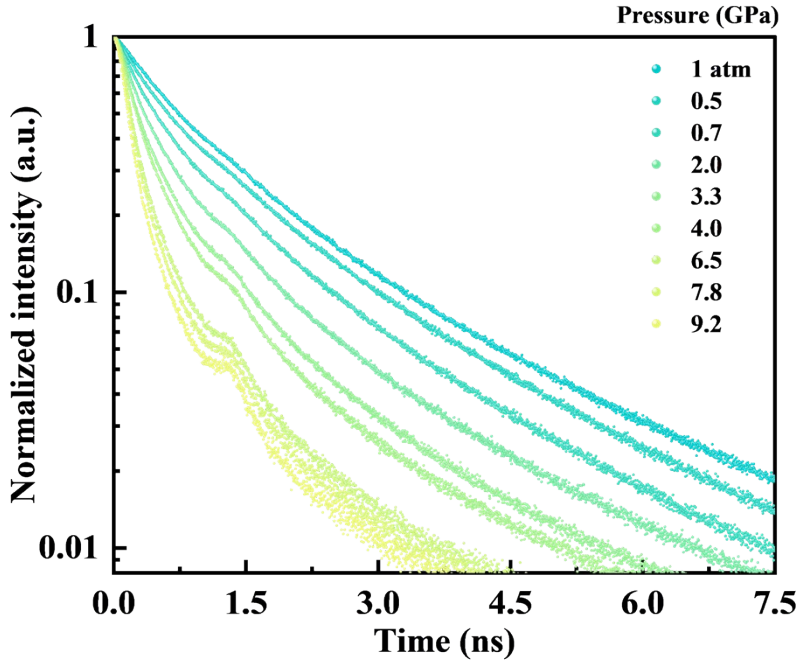

Figure S9. Normalized time-resolved PL decay curves of D-MOF upon compression

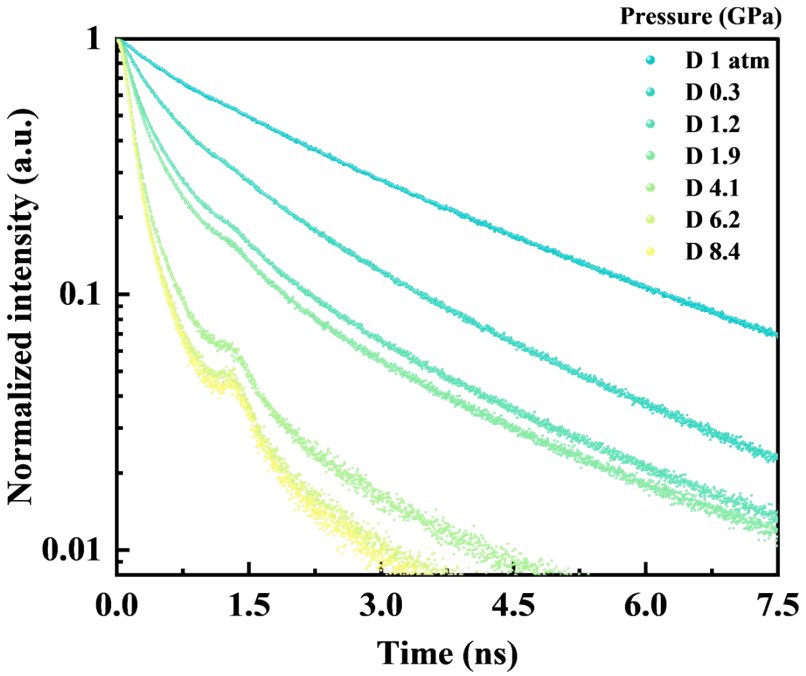

Figure S10. Normalized time-resolved PL decay curves of D-MOF during decompression.

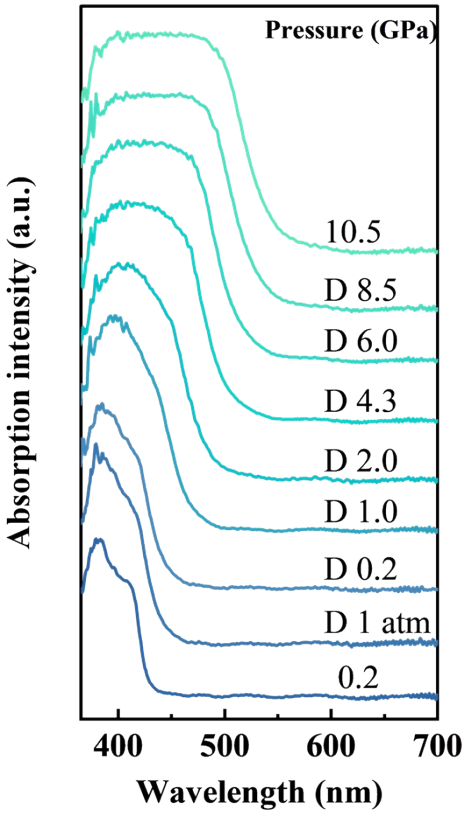

Figure S11. In-situ high-pressure UV-Vis absorption spectra of D-MOF during decompression.

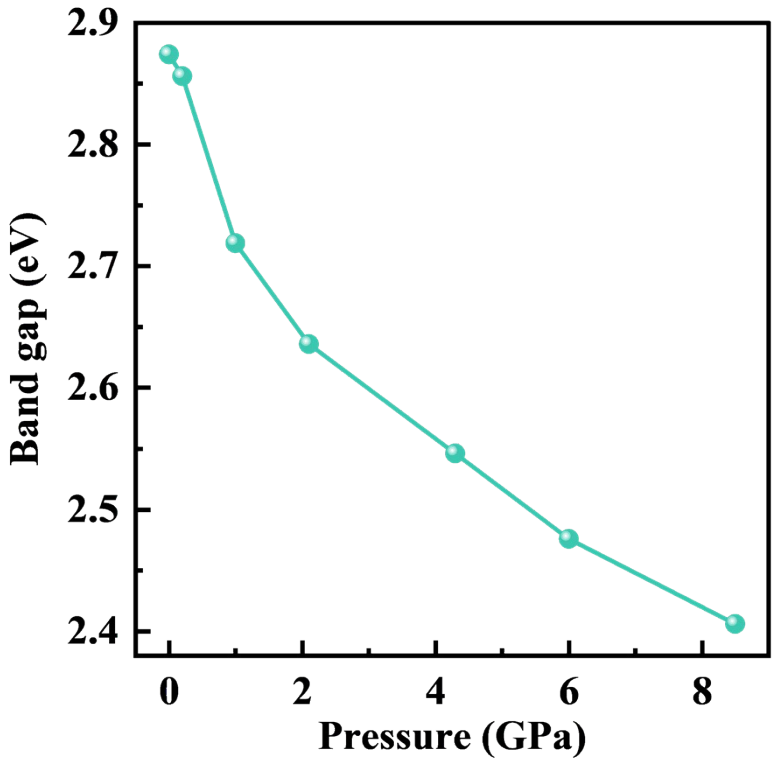

Figure S12. Pressure-dependent variation of the optical band gap of D-MOF upon decompression.

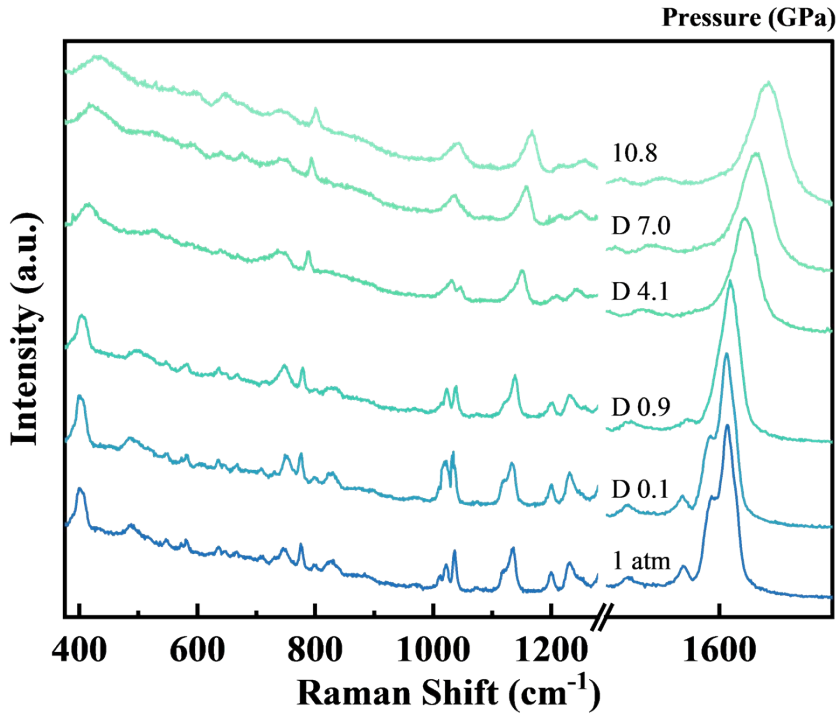

Figure S13. In-situ high-pressure Raman spectra of D-MOF during decompression.

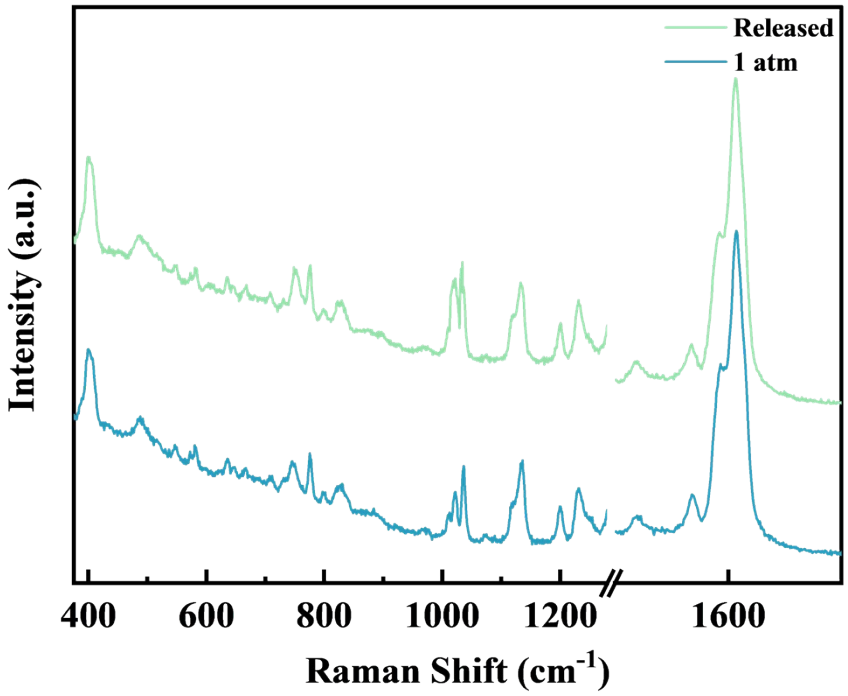

Figure S14. Comparison of in-situ Raman spectra of D-MOF at 1 atm and released from 10.8 GPa

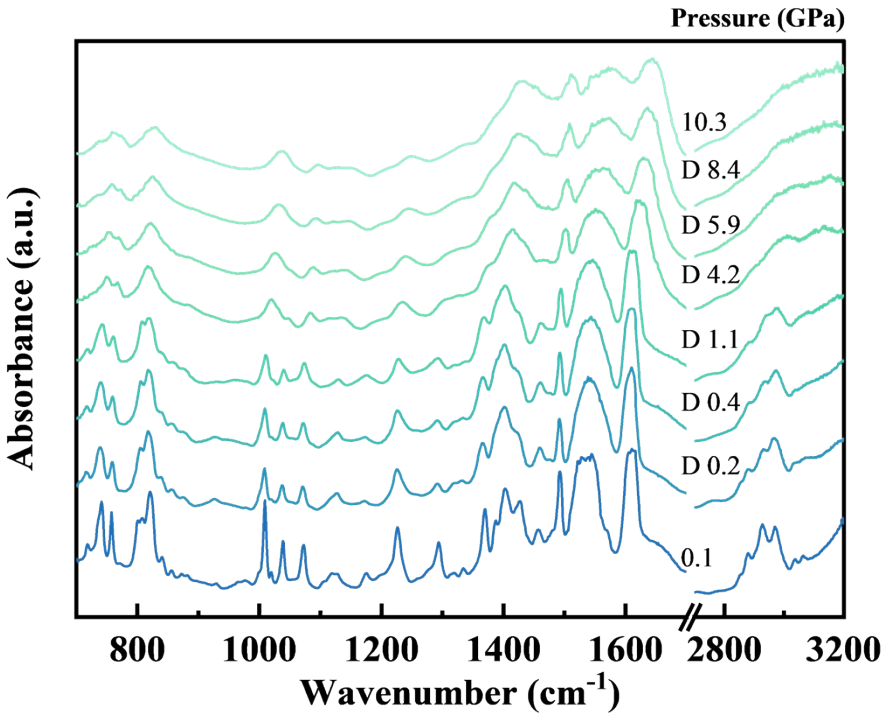

Figure S15. In-situ high-pressure IR spectra of D-MOF upon decompression.

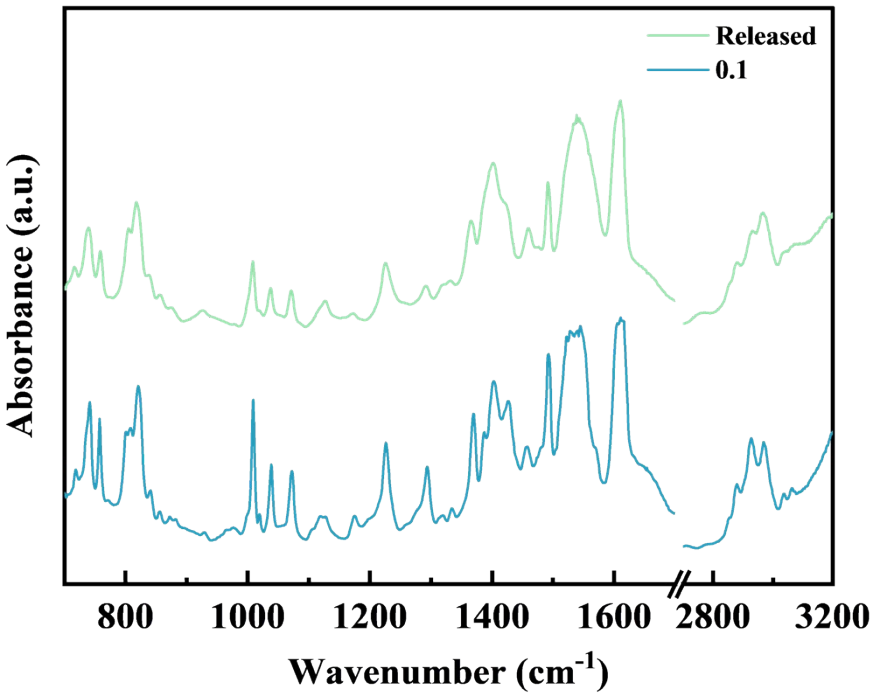

Figure S16. Comparison of in-situ IR spectra of D-MOF at 0.1 GPa and released from 10.3 GPa

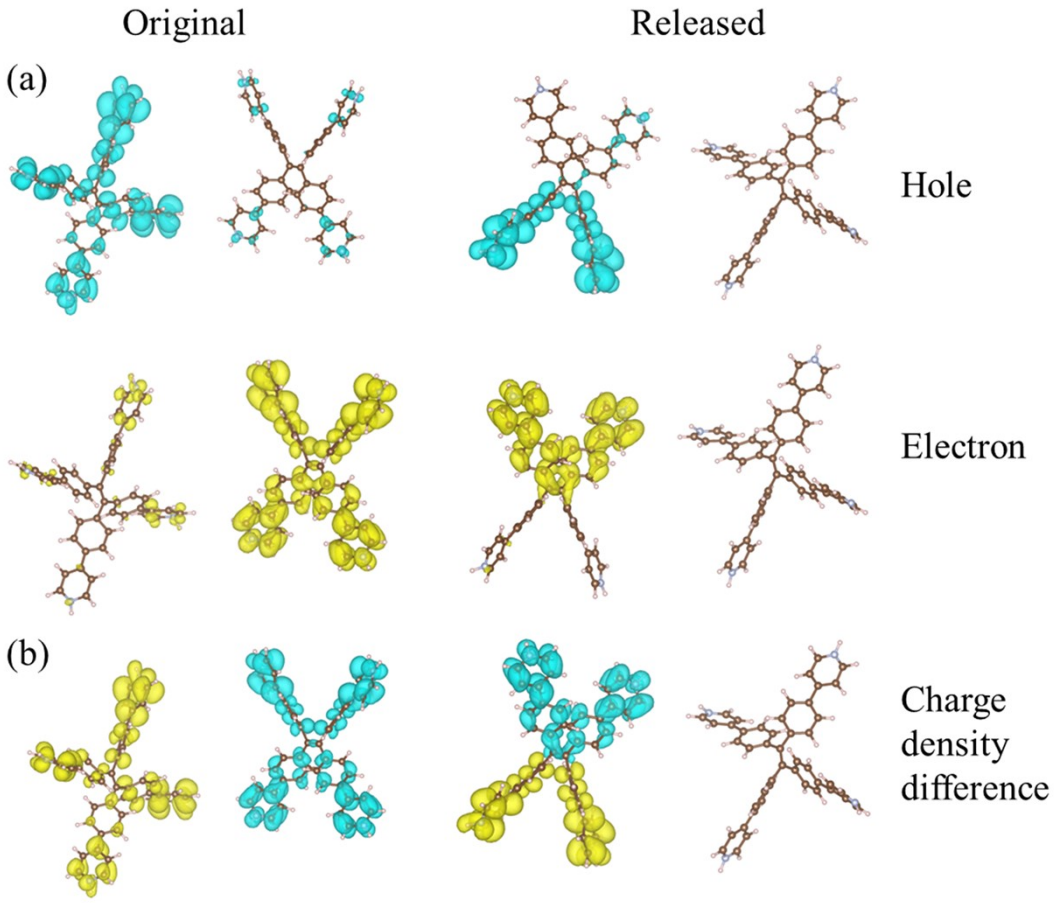

Figure S17. (a) Real space representation of hole and electron distributions of the TPPE in D-MOF under the excited state of $S_0 \rightarrow S_1$. The cyan and yellow regions denote the hole and electron distributions, respectively. (b) The difference between the charge density of excited state S_1 minus the charge density of ground state S_0. The yellow region represents the area where the charge density increases during the excitation process, while the cyan region represents the area where it decreases. The iso-value is set as 0.002.

References

1 H. K. Mao, J. Xu and P. M. Bell, *J. Geophys. Res.*, 1986, **91**, 4673–4676

2 O. V. Dolomanov, L. J. Bourhis, R. J. Gildea, J. Howard and H. Puschmann, *J. Appl. Crystallogr.*, 2009, **42**, 339–341

3 A. L. Spek, *J. Appl. Crystallogr.*, 2003, **36**, 7–13

4 A. L. Spek, *Acta Crystallogr.,* 2009, **D65**, 148–155

5 B. Delley, *J. Chem. Phys.*, 2000, **113**, 7756–7764

6 J. K. Norskov, T. Bligaard, J. Rossmeisl and C. H. Christensen, *Nat. Chem.*, 2009, **1**, 37–46

7 J. P. Perdew, K. Burke and M. Ernzerhof, *Phys. Rev. Lett.*, 1997, **78**, 1396

8 C. A. Ullrich and Z. Yang, *Braz. J. Phys.*, 2014, **44**, 154–188

9 T. D. Kuehne, M. Iannuzzi, M. Del Ben, V. V. Rybkin, P. Seewald, F. Stein, T. Laino, R. Z. Khaliullin, O. Schutt, F. Schiffmann, D. Golze, J. Wilhelm, S. Chulkov, M. H. Bani-Hashemian, V. Weber, U. Borstnik, M. Taillefumier, A. S. Jakobovits, A. Lazzaro, H. Pabst, T. Mueller, R. Schade, M. Guidon, S. Andermatt, N. Holmberg, G. K. Schenter, A. Hehn, A. Bussy, F. Belleflamme, G. Tabacchi, A. Gloss, M. Lass, I. Bethune, C. J. Mundy, C. Plessl, M. Watkins, J. Vandevondele, M. Krack and J. Hutter, *J. Chem. Phys.*, 2020, **152**, 194103

10 T. Lu and F. Chen, *J. Comput. Chem.*, 2012, **33**, 580–592

11 T. Lu, *J. Chem. Phys.*, 2024, **161**, 082503

12 K. Momma and F. Izumi, *J. Appl. Crystallogr.*, 2011, **44**, 1272–1276